Genetic determinants of penicillin tolerance in *Vibrio cholerae*

Anna I. Weaver*[1,2], Shannon G. Murphy*[1,2], Benjamin Umans[3], Srikar Tallavajhala[2], Ikenna Onyekwere[1,2], Stephen Wittels[3], Jung-Ho Shin[1,2], Michael VanNieuwenhze[4], Matthew K. Waldor[3] and Tobias Dörr[1,2#]

***contributed equally**

[1] Department of Microbiology and [2] Weill Institute for Cell and Molecular Biology, Cornell University, Ithaca, NY 14853
[3] Howard Hughes Medical Institute and Brigham and Women's Hospital/Harvard Medical School, Boston, MA 02115
[4] Department of Molecular and Cellular Biochemistry and Department of Biology, Indiana University, Bloomington, IN 47405-7003

#correspondence: tdoerr@cornell.edu

Abstract

Many bacteria are resistant to killing ("tolerant") by typically bactericidal antibiotics due to their ability to counteract drug-induced cell damage. *Vibrio cholerae*, the cholera agent, displays an unusually high tolerance to diverse inhibitors of cell wall synthesis. Exposure to these agents, which in other bacteria leads to lysis and death, results in a breakdown of the cell wall and subsequent sphere formation in *V. cholerae*. Spheres readily recover to rod-shaped cells upon antibiotic removal, but the mechanisms mediating the recovery process are not well-characterized. Here, we found that the mechanisms of recovery are dependent on environmental conditions. Interestingly, on agarose pads, spheres undergo characteristic stages during the restoration of rod shape. Drug inhibition and microscopy experiments suggest that class A Penicillin Binding Proteins (aPBPs) play a more active role than the Rod system, especially early in sphere recovery. TnSeq analyses revealed that LPS and cell wall biogenesis genes as well as the sigma E cell envelope stress response were particularly critical for recovery. LPS core and O-antigen appear to be more critical for sphere formation/integrity and viability than Lipid A modifications. Overall, our findings demonstrate that the outer membrane is a key contributor to beta lactam tolerance and suggest a role for aPBPs in cell wall biogenesis in the absence of rod-shape cues. Factors required for post-antibiotic recovery could serve as targets for antibiotic adjuvants that enhance the efficacy of antibiotics that inhibit cell wall biogenesis.

Introduction

The emergence of antibiotic resistance in bacterial pathogens requires the development of new drugs and novel strategies to combat infection. However, antibiotic resistance is not the sole explanation for antibiotic treatment failures. Instead, some infections are caused by fully susceptible pathogens that are thought to survive antibiotic treatment due to a high level of drug tolerance, i.e., the capacity to stay alive in the presence of otherwise bactericidal drugs (1-4). Dormant persister cells, which resist killing by all available antibiotics (4), represent an extreme form of antibiotic tolerance. However, susceptible (non-persister) bacteria are sometimes capable of surviving severe antibiotic-imposed damage, potentially providing an opportunity to acquire or evolve resistance mechanisms. In addition, surviving bacteria typically exhibit a prolonged lag phase after drug exposure (the post-antibiotic effect), during which they can repair antibiotic induced damage. Currently our knowledge of the molecular processes underlying antibiotic tolerance and the post-antibiotic effect is limited. Understanding the mechanistic underpinnings of post-antibiotic recovery could yield insights enabling the development of novel approaches to target tolerant organisms.

We and others have previously shown that some Gram-negative bacteria, including *Burkholderia pseudomallei, Pseudomonas aeruginosa* and *Vibrio cholerae*, the causative agent of cholera, exhibit high tolerance to ordinarily bactericidal cell wall acting antibiotics (e.g. beta lactams) (5-7). In *V. cholerae*, for

example, exposure to beta lactam antibiotics at multiples of the minimum inhibitory concentration (MIC) results in cell wall loss, similar to well-studied model organisms, such as *E. coli* (5). However, in contrast to *E. coli*, *V. cholerae* survives as wall-deficient spheres, similar to L-forms (8), with the notable difference that *V. cholerae* spheres do not divide while in this wall-less state. Remarkably, however, the wall-deficient spherical cells remain viable and have minimal plating defects on media lacking antibiotics (5). Sphere survival *in vivo* (in the mouse intestine) and *in vitro* is enabled by the two-component cell wall stress response system *wigKR* (aka *vxrAB*), which controls several processes including cell wall (peptidoglycan, PG) biosynthesis, motility, type VI secretion and biofilm formation (9-11).

The many steps in PG synthesis include cytoplasmic production of the lipid II precursor, translocation of this precursor into the periplasm, and finally precursor incorporation into the cell wall sacculus via polymerization (transglycosylation, TG) and intercrosslinking (transpeptidation, TP) reactions. TG and TP reactions are mediated by two spatiotemporally distinct entities, the Rod system (with RodA as the polymerase and a class B Penicillin Binding Protein [bPBP] as the crosslinking enzyme) and the class A PBPs (aPBPs) that can catalyze both TG and TP reactions (12). In addition, aPBPs require outer-membrane localized lipoproteins (Lpos) for their activity (13, 14) and the Rod system is associated with (and requires for its activity) the cytoskeletal actin homolog MreB (15-18). Almost the entire *V. cholerae* PG synthesis pathway is

upregulated through *wigKR/vxrAB* in response to antibiotics that disrupt cell wall synthesis (9), with the notable exception of components of the Rod system.

We have little knowledge of how *V. cholerae* cell envelope biogenesis pathways enable recovery from the antibiotic-induced spherical state and if additional factors contribute to survival and recovery from this state. Here, we have characterized the post-antibiotic recovery process in *V. cholerae*. Microscopy using fluorescent protein fusions and cell wall stains revealed that during an ordered sphere recovery process, aPBP1a localizes prominently to the outgrowth area and its function appears to account for the majority of the initial deposition of new cell wall material. In contrast, the Rod system, which is ultimately required for sphere recovery, plays a minor role in the initial recovery stages. We also used transposon insertion sequencing (TnSeq) to identify the genetic requirements for *V. cholerae* tolerance to penicillin and found that there is an enrichment in genes important for cell wall and outer membrane biogenesis functions among mutations that confer post-antibiotic fitness defects. Collectively, our findings reveal the pleiotropic nature of beta lactam tolerance, provide potential targets for beta lactam adjuvants, and have implications for the role of aPBPs in *de novo* PG template generation.

Results

Distinct mechanisms of recovery in different growth conditions

In previous work, we used microscopy to characterize *V. cholerae* sphere formation following exposure to antibiotics that interfere with cell wall synthesis

(5). Here we used a similar approach to investigate how spheres revert to rod shape. As observed previously, *V. cholerae* cells grown in minimal medium exposed to penicillin G form non-dividing spheres exhibiting well-defined demarcations between the phase-dark cytoplasm, an enlarged periplasmic space visible as a phase-light bubble, and a clearly visible outer membrane (**Fig. 1A**). Timelapse light microscopy was used to monitor cell morphology on agarose pads after removal of the antibiotic by washing. In these conditions, approximately 10 to 50% of cells fully recovered to form microcolonies (see **Movie S1** for an example). While these conditions were not as favorable for recovery as plating on LB agar (5), they enabled us to discern steps in sphere recovery, which appeared to take place in partially overlapping stages in wild type (wt) cells (**Fig. 1B).** Initially, phase dark material engulfed the periplasmic space (engulfment stage); then, the now elliptical-shaped cells reduced their widths (constriction phase) followed by elongation (elongation phase); finally these elongated cell masses gave rise to rod-shaped cells, which proliferated into a microcolony.

The pattern of recovery of rod shape described above is distinct from that described for osmostabilized, beta lactam treated *E. coli* cells (19); however the latter experiments were conducted in microfluidic chambers rather than agarose pads. Unlike *E. coli*, *V. cholerae* does not require osmostabilization for sphere formation; furthermore, *V. cholerae* spheres retain viability and structural integrity in LB and minimal medium, as well as in rabbit cecal fluid (5). Unlike the conditions in microfluidic chambers, agarose pads may provide external

structural support to recovering spheres. Consistent with this idea, we found that the pattern and dynamics of recovery were very different when we repeated recovery experiments in liquid M9 minimal medium. Following exposure to penG and washing, cells were intermittently removed from the liquid medium and imaged. We did not observe the distinct stages of recovery observed on agarose pads; in general, sphere morphology did not change for the duration of the experiment (12 h), except for a slight increase in volume (**Fig. 2**). However, normal, rod-shaped cells appeared after ~ 4-5 hours of post-antibiotic incubation (**Fig. 2**, yellow arrow). We surveyed ~ 100 cells per time point in each of two biological replicate experiments and did not find any intermediates, suggesting that if such intermediates form, they do so at a frequency <1/100. The origin of the rod-shaped cells is not clear, but they may have directly budded off of spheres from a newly-formed pole juxtaposed to the periplasm, similar to the recovery protrusions observed in *E. coli* after treatment with beta lactams (19) or lysozyme (20). Indeed, we observed some rods that appeared to be budding off of spheres (**Fig. 2**, red arrow). Thus, the morphological transitions and dynamics of sphere to rod conversion are dependent on specific culture conditions and may rely on distinct mechanisms.

PBP localization dynamics during sphere recovery

V. cholerae, like the model rod-shaped organisms *E. coli* and *B. subtilis,* encodes two distinct cell wall synthesis machineries, namely the RodAZ-MreBC-PBP2 elongation complex (Rod system) and the aPBPs (15, 21, 22). Nearly the entire

157 cell wall synthesis pathway, including aPBPs, is upregulated by the *wigKR* cell
158 wall stress response two component system. Members of the Rod system,
159 however, are conspicuously absent from the *wigKR* regulon (9). We thus
160 hypothesized that aPBPs were crucial determinants of post-antibiotic recovery.
161 To investigate the role of PBP1a, *V. cholerae*'s primary aPBP (23) in the
162 recovery process, we created a functional (**Fig. S1**) PBP1amCherry translational
163 fluorescent protein and tracked its localization in recovering spheres on agarose
164 pads. In the first stages of recovery, PBP1amCherry was diffuse, but then it
165 assumed a striking, band-like pattern along the leading edge of the periplasmic
166 engulfment, migrating ahead of the phase-dark cytoplasmic material (**Fig. 3,**
167 **yellow arrow**). Inhibiting PBP1a's TG activity using moenomycin (10 μg ml^{-1}, 10x
168 MIC), arrested sphere recovery in the pre-engulfment stage and prevented
169 proper PBP1a localization, suggesting that the recovery process depends on
170 PBP1a's PG synthesis capabilities (or at least transglycosylation function). We
171 also tested whether MreB was necessary for PBP1a's leading edge localization
172 by treating the recovering PBP1amcherry strain with the MreB inhibitor MP265
173 (24) (200 μM, 10 x MIC). Inhibition of MreB suppressed recovery and completion
174 of periplasmic engulfment, establishing that MreB is important for sphere to rod
175 recovery as shown before for *E. coli* (19). However, engulfment was only partially
176 defective in spheres treated with MP265 and PBP1a still localized in a
177 concentrated, band-like pattern in the presence of MP265 (**Fig. 3, green arrow**).
178 Thus, while both MreB and PBP1a are important for recovery, aPBPs seems to
179 function earlier than the Rod system in the process.

180

181 **The aPBPs are important for the initiation of cell wall synthesis early in**
182 **sphere recovery**

183 Since PBP1a was concentrated around the leading edge during the engulfment
184 process, we hypothesized that the aPBPs might be required for the
185 commencement of cell wall synthesis after antibiotic-induced murein degradation.
186 To test this, we treated cells with PenG, removed the antibiotic by washing, and
187 then used the fluorescent D-amino acid HADA to visualize insertion of new cell
188 wall material. An Δ*ldtA* Δ*ldtB* mutant defective in L,D transpeptidase activity (25)
189 was used in these experiments to exclude PG synthesis-independent HADA
190 incorporation. In untreated spheres, cell wall deposition generally started at the
191 opposite side of the periplasm (**Fig. 4**). This is likely the place where aPBPs and
192 their OM activators interact first, as the inner and outer membranes are in close
193 proximity in this area. In the presence of the MreB inhibitor MP265 (at 10 x MIC),
194 initial cell wall deposition was reduced compared to untreated spheres, but
195 remained detectable. In contrast, when cells were incubated with moenomycin
196 (10 x MIC), incorporation of HADA-labeled material was drastically reduced (**Fig.**
197 **4,** see **Fig. S2** for image adjusted to lower dynamic range). It follows that while
198 both the aPBPs and MreB are required for sphere recovery, the aPBPs are more
199 active than the Rod system in producing nascent PG in recovering spheres.

200

201 **Identification of genes required for post-antibiotic recovery**

We used transposon insertion site sequencing (TIS, aka TnSeq) to identify factors required for sphere recovery. Since we observed differences in recovery dynamics on solid (agarose pad) versus in liquid media, we combined both conditions in TIS experiments to uncover a broad array of recovery factors. Cells were exposed to PenG in liquid culture for 4 hr, washed, outgrown overnight in the absence of antibiotics, and then plated. The insertion sites in the Tn library were sequenced before addition of the antibiotic (PRE), after incubation in PenG (POST), and after the overnight outgrowth followed by plating (OG). Strikingly, comparison of the insertion profiles in the PRE and POST conditions (**Fig. 5A**) did not reveal any genes that met stringent criteria for differential fitness (>10-fold difference in insertion abundance, p-val <0.01). Thus, no single mutation appears to lead to catastrophic lysis in *V. cholerae* treated with penicillin G. In contrast, comparing the insertion profiles in the POST vs OG conditions revealed 55 genes which had reduced fitness during post-antibiotic outgrowth (>10-fold fewer insertions along with p-val <0.01).

Notably, there was an enrichment of several functional pathways among the 55 genes required for robust post-antibiotic outgrowth (**Fig. 5B**). Included among the enriched categories were genes predicted to be required for cell wall synthesis and recycling (*pbp1A*, *vc2153*, *ampG, pbp5*, *lpoB*, *mltA*), lipopolysaccharide (LPS) biosynthesis (core biosynthesis, Lipid A acylation and O-antigen synthesis pathways, *vc0212, vc0223, vc0225, vc0236, vc0237, vc0240*), intrinsic stress resistance (superoxide dismutase, *rpoE*), phosphate uptake (*vc0724-0726*) and chromosome dynamics (*mukBEF*) (**Fig. S3)**.

225 Intriguingly, some of the hits (*vc2153*, *rpoE*, PG synthesis factors) were
226 homologs or analogs of factors identified in a recent TnSeq screen for genes that
227 promote tolerance to beta lactams in *Burkholderia pseudomallei* and *B.*
228 *thailandensis* (6), raising the possibility that there are shared tolerance
229 requirements across Gram-negative bacteria.

230 We were particularly interested in the contribution of cell envelope
231 functions to sphere recovery and therefore prioritized genes involved in LPS and
232 cell wall metabolism for further studies. We first focused on the 6 LPS
233 biosynthesis genes that answered our screen. To validate the requirement of
234 LPS core biosynthesis in the recovery process, we created an insertion mutant in
235 *vc0225,* the gene encoding heptosyltransferase I. This mutation is expected to
236 result in a truncated LPS molecule lacking an outer core and O-antigen and
237 consistent with this, the mutant strain did not have detectable high molecular
238 weight LPS in isolated outer membrane (OM) material (**Fig. S4**). Wild type (wt)
239 and *vc0225::kan* mutant cells were compared in time-dependent viability
240 experiments. Exposing wt cells to penicillin G (at 10 x MIC) in minimal medium
241 (unlike LB) in some experiments permitted initial growth (**Fig. 6A**). We do not
242 know the reason for this initial growth (*V. cholerae* does not become resistant to
243 PenG in M9, as evidenced by sphere formation (**Fig. 6B**), but it is possible that
244 antibiotic diffusion through the OM is slower in minimal than in rich medium.
245 Disruption of the LPS core gene *vc0225* resulted in the absence of initial growth
246 and a subsequent 100-fold plating defect after exposure to PenG (**Fig. 6A**),
247 corroborating the TnSeq result. This survival defect could be complemented by

248 expressing *vc0225* from a neutral chromosomal locus. Light microscopy revealed
249 that the *vc0225* mutant strain still formed spheres (**Fig. 6B**); however, these
250 spheres were morphologically distinct from wt spheres. In contrast to wt
251 spheres, which were usually seen as single cells, exhibiting well-demarcated
252 separation between the phase dark cytoplasm and the phase light periplasm
253 (**Fig. 1A**), *vc0225* mutant cells were mostly grape-like masses showing a
254 checkered pattern of distinct periplasmic enclaves in a sometimes divided
255 cytoplasm (**Fig. 6B**). Visualizing an inner membrane marker (PBP1amCherry)
256 also revealed the lack of a clear distinction between the inner and outer
257 membrane in the mutant. Upon removal of the antibiotic, *vc0225* spheres were
258 defective in all stages of the recovery process; the spheres underwent modest
259 enlargement without initiating periplasmic engulfment (**Fig. 6C**). Thus, intact LPS
260 appears necessary for sphere anatomy and internal organization; moreover,
261 these LPS-associated sphere defects seem to impair sphere recovery.
262
263 **Sphere integrity does not depend on Lipid A modifications**
264 The outer membrane appears to be the principle load-bearing structure in beta
265 lactam-induced spheres, because these cells are largely devoid of detectable cell
266 wall material and are more susceptible to detergents and antimicrobial peptides
267 (5, 7). *V. cholerae* LPS contains at least two modifications which are not found in
268 *E. coli* LPS and that could potentially stabilize *V. cholerae* spheres. These
269 modifications, addition of phosphoethanolamine to the 1-phosphate group of lipid
270 A and an unusual glycine addition to a hydroxylauryl chain at the 2' position of

Lipid A, both promote resistance to polymyxin (26, 27); glycinylation (by the *alm* system) is dominant, but the pH-dependent EptA can promote residual polymyxin resistance when the *alm* system is inactivated (22). We investigated whether these modifications were required for sphere formation and integrity by deleting the *alm* operon, which encodes the glycine transferase activity, and *eptA*, which encodes the ethanolamine transferase. As expected, the *alm* mutation abrogated polymyxin resistance on LB (**Fig. S5**). When these mutants, either alone (not shown) or in combination, were exposed to PenG they formed spheres that were indistinguishable from wt spheres (**Fig. 7A**), indicating that these Lipid A modifications are not required for sphere generation. The Δ*alm* Δ*eptA* mutations were then combined with disruptions in *vc0225* or *vc0212* (encoding the 3-hydroxy laurate transferase LpxN (28)) to test the effect of a core mutation (*vc0225*) or Lipid A under-acylation (*vc0212*) on sphere formation in LPS lacking glycine and ethanolamine modifications. (Note that mutation of *lpxN* results in the absence of the acyl chain modified by glycine and thus causes polymyxin B sensitivity, **Fig. S5**). The ΔalmΔeptA *vc0212::kan* mutant still formed spheres after PenG exposure (**Fig. 7A**) but these spheres had ~5-fold decrease in viability compared to the wt (**Fig. 7B**). The Δ*alm* Δ*eptA vc0225::kan* mutant also formed spheres, but resulted in a more dramatic reduction in viability compared to the Δ*alm*Δ*eptA vc0212::kan* mutant (**Fig. 7B**) and to the single *vc0225::kan* mutant , where there was less pronounced loss of viability after 3 h (compare with **Fig. 6A**). Thus, LPS core and O-antigen appear to be more critical for sphere formation/integrity and viability than Lipid A modifications. However,

glycinylation and/or ethanolamine addition to Lipid A appear to promote maintenance of sphere integrity in the absence of LPS core and O-antigen, suggesting that these modifications contribute to OM stability in this context.

The sigma E cell envelope stress response is required for penicillin tolerance

The TnSeq analysis implicated several genes in the sigma E cell envelope stress response as important for sphere viability/recovery (**Fig. S3**). Misfolding of outer membrane proteins such as OmpU triggers the *V. cholerae* envelope stress response, wherein sigma E directs the transcription of a set of genes involved in variety of cell envelope maintenance functions (29, 30). We found that the abundance of RpoE markedly increased several hours after cells were exposed to diverse antibiotics that interrupt cell wall synthesis (PenG, phosphomycin or D-cycloserine), consistent with the idea that this sigma factor promotes sphere survival (**Fig. 8A)**. Interestingly, PenG treatment increased RpoE abundance independent of OmpU (**Fig. 8B**). The importance of sigma E for survival after PenG exposure was established by measuring time-dependent viability after antibiotic challenge. Since *rpoE* is essential, we used an Δ*rpoE*Δ*ompU* strain (the latter deletion enables *rpoE* deletion (30)), to investigate *rpoE*'s importance for sphere viability/recovery. Following exposure to PenG, the Δ*rpoE*Δ*ompU* strain exhibited a drastic (~1000-fold) plating defect compared to the wild type and Δ*ompU* controls (**Fig. 8B**). Thus, sigma E (and presumably the regulon it controls) is a crucial determinant of *V. cholerae* beta lactam tolerance.

317 The importance of the sigma E response for beta lactam tolerance
318 indicated the strong possibility that PenG-treated *V. cholerae* sustain OM
319 damage; this in turn suggested that beta lactam exposure might sensitize cells to
320 high molecular weight (HMW) antibiotics that are typically too large to permeate
321 the Gram-negative cell envelope; e.g. vancomycin and ramoplanin. To test this,
322 we plated cells exposed to PenG or a vehicle control on either LB or plates
323 containing vancomycin (100 μg ml^{-1}) or ramoplanin (100 μg ml^{-1} and 500 μg ml^{-1})
324 (**Fig. 8C)**. While untreated cultures plated at close to 100% on any of these
325 plates, pre-treatment with PenG for 3h resulted in a 10- to 50-fold plating defect
326 on either HMW antibiotic. Thus, while *V. cholerae* is tolerant to beta lactam
327 antibiotics, these agents appear to sensitize it against HMW antibiotics.
328

329 # Discussion

330 Antibiotic tolerance, the ability to survive and fully recover from exposure to
331 normally lethal doses of bactericidal antibiotics, is a common cause of treatment
332 failure and serves as a stepping-stone for the development of antibiotic
333 resistance (31). The mechanism(s) of antibiotic tolerance and a related
334 phenomenon, the post-antibiotic effect (the recovery process of tolerant cells) are
335 understudied and insufficiently understood.
336 Here, we investigated the post-antibiotic effect in *V. cholerae,* an organism
337 highly tolerant to typically bactericidal inhibitors of cell wall synthesis. Following
338 beta lactam treatment, this pathogen forms viable cell wall deficient spheres that
339 can re-establish their characteristic rod morphology when antibiotics are no

longer present. We found that the process of restoration of rod shape appears to be media dependent and to differ from that described for the recovery of *E. coli* spheres induced by cefsulodin (19). At least on agarose pads, 3 successive steps characterized the recovery process. Recovery involves re-localization of PBP1a to the leading edge of a periplasmic engulfment process and aPBPs, rather than the Rod system, have a primary role, particularly in the early steps of recovery. The characteristic steps and protein localization patterns involved in restoration of rod shape suggests that *V. cholerae*'s ability to recover from a well-less spherical state may be a previously unappreciated type of programmed response to stress. Furthermore, the capacity of wall-less spheres to remain viable and to regain rod shape in a step-wise fashion is not restricted to *V. cholerae*, but found in several other Gram-negative organisms (7, 20, 32).

Not surprisingly, TnSeq analysis revealed that genes required for peptidoglycan biogenesis were essential for sphere recovery; however, additional envelope-related functions, particularly LPS biosynthesis, and the RpoE envelope stress response system were also critical for *V. cholerae* spheres to recover from beta lactam assault. While this TnSeq dataset offers many intriguing leads for future studies of the post-antibiotic recovery process (e.g. the role of riboflavin and condensins), here we primarily focused on the role of LPS and PG biosynthesis in role.

Mutations in LPS core and O-antigen biosynthesis can have at least two potentially detrimental consequences for sphere viability/recovery. First, truncated (rough) LPS has been shown to result in increased OM permeability

363 due to the surface presentation of phospholipid bilayer patches resulting from
364 LPS instability (33). Second, truncated LPS, which cannot be ligated to O-
365 antigen, results in the accumulation of dead-end intermediates of O-antigen
366 fused to the lipid carrier molecule undecaprenol (UNDP) (34). UNDP
367 concentrations are limited and this carrier is critical for the biosynthesis of a
368 variety of extracellular macromolecules, including peptidoglycan. Thus, in
369 addition to direct effects on OM integrity, LPS core mutations can also impede
370 efficient cell wall synthesis due to the reduced availability of UNDP; the
371 consequences of such inhibition may be particularly severe for PG-deficient
372 spheres. However, LPS core mutants exhibited post-antibiotic exposure
373 phenotypes that cannot easily be explained by cell wall precursor depletion
374 alone. The absence of the clear demarcation between the inner and outer
375 membrane in the LPS core (*vc0225* mutant) deficient spheres suggests that IM
376 material (IM phospholipids and associated proteins) may be present in the OM.
377 More broadly, our findings demonstrate the importance of LPS integrity for *V.*
378 *cholerae* survival of cell wall damage; it is likely that LPS structure/strength
379 modulates susceptibility to beta lactams in other bacteria as well, as has been
380 suggested in *E. coli* (35).

381 As expected, we also found cell wall synthesis and recycling factors to be
382 required for sphere recovery. The prominent role of PBP1a, rather than its
383 paralog PBP1b, in the recovery process supports our previous data showing that
384 PBP1a is the principle aPBP in *V. cholerae* (23, 36) and is consistent with
385 observations in lysozyme-treated, spherical *E. coli*, where that organism's

386 principal aPBP (PBP1B) is required for recovery (32). Intriguingly, PBP1a
387 localized as a concentrated ring around the outgrowth area. Moenomycin, an
388 aPBP TG inhibitor, abrogated PBP1a's capacity to localize to the outgrowth area
389 as well as sphere recovery, revealing the essentiality of aPBP enzymatic activity
390 for the recovery process. In contrast, MreB, and by extension likely the
391 associated Rod system appeared to play a minor role during the early stages of
392 recovery (though MreB was ultimately necessary for full sphere-to-rod
393 conversion). We do not know the exact structure of possible remnant PG in
394 spheres; however, our results suggest that aPBPs are more efficient than the
395 Rod system at starting PG synthesis in the absence of a rod-shaped scaffold.
396 Recent data suggest that MreB determines the directionality of Rod-mediated PG
397 synthesis through its axial, membrane-curvature-induced orientation in the cell
398 (37). Our data are in line with such a model, as axial localization cues are lost in
399 a sphere. Thus, the Rod system might rely on the aPBPs to first mediate some
400 degree of sphere constriction, inducing heterogeneity in membrane curvature
401 that would then enable ordered, Rod-mediated PG deposition resulting in cell
402 elongation.

403 In summary, we provide here an analysis of factors required for post-
404 antibiotic recovery in *V. cholerae* treated with a beta lactam antibiotic. Our results
405 directly demonstrate a role for OM integrity in beta lactam tolerance and establish
406 a differential role for aPBPs and the Rod system for post-antibiotic recovery. The
407 factors identified here could serve as novel targets for antibiotic adjuvants that

increase the efficacy of beta lactam antibiotics and other inhibitors of cell wall synthesis towards Gram-negative pathogens.

Acknowledgements

We thank Hongbaek Cho and Thomas Bernhardt for the msfGFP template. Carol Gross is acknowledged for her gift of the anti RpoE antibody. Research in the Waldor lab is supported by the Howard Hughes Medical Institute and NIH (2R01-AI-042347-23). Research in the VanNieuwenhze lab is supported by NIH grant GM113172.

Materials and Methods

Media, chemicals and growth conditions

All growth experiments were conducted either in Luria Bertani Broth (LB) or M9 minimal medium supplemented with glucose (0.2 %). Antibiotics were purchased from the following suppliers: Moenomycin (Santa Cruz), MP265 (Santa Cruz) Penicillin G (Fisher), streptomycin (Santa Cruz). Unless otherwise noted, all experiments were conducted in three biological replicates (i.e. experiments conducted on different days). For each experiment, two independent overnight cultures were used; where possible (i.e. for mutants constructed in this study) these cultures were inoculated from two independently isolated clones.

Molecular techniques/strain construction

For molecular cloning purposes, PCR was conducted using Q5 high fidelity polymerase (NEB). For diagnostic PCRs, OneTaq mastermix (NEB) was used instead. All cloned constructs were verified using sequencing. All plasmid cloning was done using Isothermal Assembly (ITA) (38). Oligos are summarized in **Table S1** and strains in **Table S2**. Unless otherwise noted, all strains were constructed in the El Tor N16961 background.

Unless otherwise noted, mutants were constructed as previously described using the suicide plasmid pCVD442 (39) and homologous recombination to replace genes with the sequence TAATGCGGCCGCACTCGAGTAATAATGATGA. Briefly, the *E. coli* donor strain Sm10 carrying a pCVD-based deletion plasmid was mixed 1:1 with the *V. cholerae* recipient on an LB plate and incubated for at least 2h at 37 ˚C. The cell mixture was then streaked out on a plate containing carbenicillin (100 µg/ml) and streptomycin (200 µg/ml) to select against the donor strain and for recipients that have integrated the deletion plasmid. To counterselect against pCVD, a single colony was then streaked out on sucrose agar (15 g/L agar, 10 g/L tryptone, 5 g/L yeast extract, filter-sterilized sucrose added after autoclaving to 10 % final concentration) + streptomycin. Plates were incubated at ambient temperature for 1 day and then transferred to 30 ˚C, followed by additional incubation for 1 or 2 days. Successful mutants were verified via colony PCR using primers flanking the gene of interest.

453 For the *vc0225* disruption, *sacB*-based counterselection did not work due to the
454 inability of LPS core mutants to grow on sucrose agar. We therefore used a kanR
455 (conferring kanamycin reistance) variant of the single crossover suicide vector
456 pGP704 (40) to create insertion disruption mutants. To this end, a 400bp internal
457 fragment (nucleotide position 27 – 427) of *vc0225* or a 461 bp internal fragment
458 (nucleotide position 93 – 554) of *vc0212* was cloned into pGPkan and transferred
459 into recipient *V. cholerae* using the di-amino pimelic acid (DAP)-auxotrophic *E.*
460 *coli* donor strain MFD lambda pir (41). Insertion mutants were selected on plates
461 containing streptomycin (200 µg/ml) and kanamycin (50 µg/ml).
462 Procedures for the construction of other knockout plasmids and strains was as
463 follows:
464
465 *Pbp1a::pbp1amcherry*
466 Upstream and downstream regions were amplified using primers TDP 1362/1434
467 and TDP 1435/232 respectively and fused with mCherry (amplified using primers
468 1436/1437) and Xba1-digested pCVD442 using ITA. These primers insert the
469 linker sequence gacatcctcgagctc between PBP1a (no stop codon) and mCherry.
470 Δ*alm* Δ*eptA*
471 For the Δ*alm* plasmid, upstream and downstream homologies were amplified
472 using primers 519/520 and 521/522 respectively. For Δ*eptA*, upstream and
473 downstream homology regions were amplified using primers 539/540 and
474 541/542.
475

476 **TnSeq**

477 TnSeq was conducted as described before (42-44); briefly, cultures were
478 subjected to transposon (mariner) mutagenesis in duplicate. In the resulting
479 libraries (~200,000 colonies/replicate), whle population transposon-chromosome
480 junctions were sequenced (PRE sample, see below); the libraries were then
481 frozen down in 30 % glycerol (-80˚C). For the experiment, libraries were grown to
482 an OD600 ~0.5 then exposed to penicillin G (100 µg/ml, 10 x MIC) for 4 h and
483 sequenced again (POST sample), followed by washing to remove the antibiotic
484 and outgrowth overnight; after which the libraries were sequenced again
485 (outgrowth, OG sample). Sequencing was performed as follows. Pelleted
486 libraries were lysed and DNA fragmented using NEB fragmentase, followed by
487 blunting (Blunting enzyme mix, NEB), A-tailing and ligation of specific adaptors.
488 Transposon-DNA junctions were then PCR amplified using transposon- and
489 adaptor-specific primers. The libraries were then sequenced on an Illumina
490 MiSeq. Data analysis was essentially conducted as described (42-44), however,
491 to avoid false negatives that did not pass our stringent cut-off, we also used a
492 candidate-based approach (based on known genetic interactions between cell
493 envelope functions) to visually inspect the TnSeq dataset in the genome browser
494 Artemis (this approach yielded e.g. WigKR and RpoE).
495

496 **Recovery on agarose pads**

497 For recovery timelapses, overnight cultures were diluted 100-fold into fresh M9
498 MM, then grown until OD600 = 0.3 (3.5 h) at 37 ˚C shaking. Antibiotic was then

added, followed by incubation for another 3h. Cells were then washed twice in antibiotic-free medium and applied to agarose patches (0.8 % agarose in M9) and imaged every 5 min on a Leica DMi8 inverted microscope with incubated (30 ˚C) stage. For fluorescent readings, exposure time was 500 ms (mCherry), 300 ms (msfGFP) or 1000 ms (HADA).

Recovery in liquid medium

Overnight cultures were diluted 100fold into fresh M9 MM, then grown until OD600 = 0.3 (3.5 h) at 37 ˚C shaking. Antibiotic was then added, followed by incubation for another 3h. Cells were then washed twice in antibiotic-free medium and diluted 10fold into same containing 100 µM HADA. Cells were withdrawn at the indicated time points, washed once with M9 and imaged as detailed above.

Figure legends

Figure 1. Recovery of *V. cholerae* rod morphology on agarose pads. A) Sphere anatomy after 3 h of treatment with PenG. OM, outer membrane, IM, inner membrane, C, cytoplasm, P, periplasm. Cellular compartments as determined in (5) using fluorescent protein fusions with known localization patterns. Scale bar = 1 µm B) Representative timelapse images of PenG-generated spheres after removal of the antibiotic on an agarose pad.

Figure 2. Sphere recovery in liquid medium. Cells were grown to a density of ~ 2 x 10^8 cfu/ml (T0) in minimal medium, exposed to penicillin G (100 µg ml^{-1}, 10x MIC) for 3 h (T3), then washed twice to remove the antibiotic and then imaged every hour. Yellow arrowheads show rod shaped cells and red arrowhead (plus enlarged window) shows sphere apparently budding of a rod.

Figure 3. PBP1a localizes to the leading edge of engulfment during sphere recovery. Cells were exposed to PenG (µg ml^{-1}, 10 x MIC) for 3 h, followed by washing and application to agarose pads containing either no antibiotic, the aPBP inhibitor moenomcyin or the MreB inhibitor MP265 (both at 10x MIC). Frames are 10 min apart, scale bar = 5 µm. Arrows point to examples of ring-like localization of PBP1a in untreated spheres (yellow arrow) or those exposed to MP265 (green arrow).

Figure 4. Deposition of new cell wall material in recovering spheres is primarily mediated by aPBPs. N16961 Δ*ldtA* Δ*ldtB* cells were exposed to PenG (100 µg ml^{-1}, 10 x MIC) in M9 minimal medium for 3 h (T0 and T3), followed by washing and resuspension in fresh, pre-warmed M9 containing the fluorescent D-amino acid analog HADA as a cell wall label (4-12 h). Scale bar = 5 µm. The MreB inhibitor MP265 was added at 200 µM (10 x MIC) and the aPBP inhibitor moenomycin at 10 µg ml^{-1} (10x MIC).

Figure 5. Identification of genes required for sphere recovery with TnSeq. **A)** Schematic of experimental design and volcano plots of change in relative abundance of insertion mutants between the two conditions (x axis) vs the concordance of independent insertion mutants within each gene (y axis, inverse p-value). The square denotes the cutoff criteria applied (>10-fold fitness defect, p-value <0.01) for identification of genes contributing to sphere recovery. PRE vs POST is a comparison of insertion frequencies after/before antibiotic exposure; POST vs. OG between an outgrowth period and directly after antibiotic exposure (see Methods for details) **B)** Distribution of the main functional categories of gene insertions that confer a post-antibiotic fitness defect. Functional categories were assigned manually following annotation of individual proteins in the Kegg database (http://www.genome.jp/kegg/).

Figure 6. An LPS core mutant is defective in sphere recovery and organization. A) Time-dependent viability experiment in the presence of PenG. Strains were exposed to PenG (100 μg ml^{-1}, 10x MIC) at T0 and plated for cfu ml^{-1} at the indicated times. **B)** Localization of Penicillin Binding Protein 1a (PBP1a) in PenG-treated wt (top) and mutant spheres (bottom). PBP1amCherry was expressed from its native, chromosomal locus. Scale bar = 5 μm **C)** Recovery pattern in a PenG-treated PBP1amCherry *vc0225* mutant after exposure to and subsequent removal of PenG. Frames are 10 min apart.

565 **Figure 7. Outer membrane modifications are not required for sphere**
566 **formation. A)** Sphere formation in wt and mutants defective in glycine (*alm*) and
567 ethanolamine (*eptA*) modifications alone and in combination with defects in LPS
568 core biosynthesis (*vc0225*) and lipid A acylation (*vc0212*). Scale bar = 5 μm **B)**
569 Time-dependent viability experiment as described in **Fig 4A**.
570
571 **Figure 8. Sigma E is induced in response to cell wall acting antibiotics and**
572 **is required for beta lactam tolerance.**
573 **A)** Western Blot using anti-RpoE antiserum after exposure to penicillin G (PenG,
574 100 μg ml^{-1}, 10x MIC), phosphomycin (phospho, 100 μg ml^{-1}, 3 x MIC) or D-
575 cycloserine (D-cyc, 100 μg ml^{-1}, 3 x MIC). **B)** Time-dependent viability of
576 indicated strains after exposure to PenG (100 μg ml^{-1}, 10 x MIC). **C)**
577 Pretreatment with PenG sensitizes cells to high molecular weight antibiotics.
578 Cells were exposed to either vehicle (no pretreatment) or Penicillin G (PenG, 100
579 μg ml^{-1}) for 3h, followed by plating on either LB, vancomycin (vanco, 200 μg ml^{-1}),
580 or ramoplanin (ramo, 100 μg ml^{-1} or 500 μg ml^{-1}).
581
582
583 **Figure S1.** Fluorescent protein fusion to PBP1a is functional. Overnight cultures
584 of the indicated strains were plated on LB agar containing 100 μg ml^{-1} cefsulodin,
585 an inhibitor of PBP1B (23).
586

587 **Figure S2.** HADA staining in recovering spheres treated with inhibitors of aPBPs
588 or the Rod system. Frames are taken from the experiment as shown in **Figure 4.**
589 The pixel intensity range was set to 100 – 2000 in all images to illustrate the
590 above background fluorescence in moenomycin-treated cells. Note that this
591 results in overexposure of the untreated sample image.
592
593 **Figure S3. A)** TnSeq hits below the cutoff (>/= 10-fold fitness defect, p-val <
594 0.01). **B)** representative Artemis plots of the genes encoding Heptosyltransferase
595 I (*vc0225)* and the Sigma E operon. POST results from analyses Post-antibiotic;
596 OG results from analyses after post-antibiotic outgrowth.
597
598 **Figure S4.** Silver stain of *V. cholerae* isolated outer membranes, comparing wild
599 type and the *vc0225* mutant. The red arrow points to high molecular weight
600 structures, likely core + O-antigen, M, marker.
601
602 **Figure S5.** Polymyxin sensitivity of *alm* and *eptA* mutants. Overnight cultures of
603 the indicated strains were plated on LB agar containing Polymyxin B at 10 μg ml^{-1}
604 and IPTG (100 μM) where applicable.
605
606 **Movie S1.** Representative timelapse of wt *V. cholerae* sphere recovery. Cells
607 were exposed to PenG in M9 MM + glucose, followed by washing and transfer to
608 an agarose pad containing M9 MM + glucose. Frames are 5 min apart.
609

1. Meylan S, Andrews IW, Collins JJ. 2018. Targeting Antibiotic Tolerance, Pathogen by Pathogen. Cell 172:1228-1238.
2. Conlon BP, Rowe SE, Lewis K. 2015. Persister cells in biofilm associated infections. Adv Exp Med Biol 831:1-9.
3. Sharma B, Brown AV, Matluck NE, Hu LT, Lewis K. 2015. Borrelia burgdorferi, the Causative Agent of Lyme Disease, Forms Drug-Tolerant Persister Cells. Antimicrob Agents Chemother 59:4616-24.
4. Lewis K. 2010. Persister cells. Annu Rev Microbiol 64:357-72.
5. Dorr T, Davis BM, Waldor MK. 2015. Endopeptidase-mediated beta lactam tolerance. PLoS Pathog 11:e1004850.
6. Held K, Gasper J, Morgan S, Siehnel R, Singh P, Manoil C. 2018. Determinants of Extreme beta-Lactam Tolerance in the Burkholderia pseudomallei Complex. Antimicrob Agents Chemother 62.
7. Monahan LG, Turnbull L, Osvath SR, Birch D, Charles IG, Whitchurch CB. 2014. Rapid conversion of Pseudomonas aeruginosa to a spherical cell morphotype facilitates tolerance to carbapenems and penicillins but increases susceptibility to antimicrobial peptides. Antimicrob Agents Chemother 58:1956-62.
8. Errington J, Mickiewicz K, Kawai Y, Wu LJ. 2016. L-form bacteria, chronic diseases and the origins of life. Philos Trans R Soc Lond B Biol Sci 371.
9. Dorr T, Alvarez L, Delgado F, Davis BM, Cava F, Waldor MK. 2016. A cell wall damage response mediated by a sensor kinase/response regulator pair enables beta-lactam tolerance. Proc Natl Acad Sci U S A 113:404-9.
10. Cheng AT, Ottemann KM, Yildiz FH. 2015. Vibrio cholerae Response Regulator VxrB Controls Colonization and Regulates the Type VI Secretion System. PLoS Pathog 11:e1004933.
11. Teschler JK, Cheng AT, Yildiz FH. 2017. The Two-Component Signal Transduction System VxrAB Positively Regulates Vibrio cholerae Biofilm Formation. J Bacteriol 199.
12. Zhao H, Patel V, Helmann JD, Dorr T. 2017. Don't let sleeping dogmas lie: new views of peptidoglycan synthesis and its regulation. Mol Microbiol 106:847-860.
13. Typas A, Banzhaf M, van den Berg van Saparoea B, Verheul J, Biboy J, Nichols RJ, Zietek M, Beilharz K, Kannenberg K, von Rechenberg M, Breukink E, den Blaauwen T, Gross CA, Vollmer W. 2010. Regulation of peptidoglycan synthesis by outer-membrane proteins. Cell 143:1097-109.
14. Paradis-Bleau C, Markovski M, Uehara T, Lupoli TJ, Walker S, Kahne DE, Bernhardt TG. 2010. Lipoprotein cofactors located in the outer membrane activate bacterial cell wall polymerases. Cell 143:1110-20.
15. Cho H, Wivagg CN, Kapoor M, Barry Z, Rohs PD, Suh H, Marto JA, Garner EC, Bernhardt TG. 2016. Bacterial cell wall biogenesis is mediated by SEDS and PBP polymerase families functioning semi-autonomously. Nat Microbiol doi:10.1038/nmicrobiol.2016.172:16172.
16. Garner EC, Bernard R, Wang W, Zhuang X, Rudner DZ, Mitchison T. 2011. Coupled, circumferential motions of the cell wall synthesis machinery and MreB filaments in B. subtilis. Science 333:222-5.

17. Dominguez-Escobar J, Chastanet A, Crevenna AH, Fromion V, Wedlich-Soldner R, Carballido-Lopez R. 2011. Processive movement of MreB-associated cell wall biosynthetic complexes in bacteria. Science 333:225-8.
18. van Teeffelen S, Wang S, Furchtgott L, Huang KC, Wingreen NS, Shaevitz JW, Gitai Z. 2011. The bacterial actin MreB rotates, and rotation depends on cell-wall assembly. Proc Natl Acad Sci U S A 108:15822-7.
19. Billings G, Ouzounov N, Ursell T, Desmarais SM, Shaevitz J, Gitai Z, Huang KC. 2014. De novo morphogenesis in L-forms via geometric control of cell growth. Mol Microbiol 93:883-96.
20. Ranjit DK, Young KD. 2013. The Rcs stress response and accessory envelope proteins are required for de novo generation of cell shape in Escherichia coli. J Bacteriol 195:2452-62.
21. Morgenstein RM, Bratton BP, Nguyen JP, Ouzounov N, Shaevitz JW, Gitai Z. 2015. RodZ links MreB to cell wall synthesis to mediate MreB rotation and robust morphogenesis. Proc Natl Acad Sci U S A 112:12510-5.
22. Lee TK, Meng K, Shi H, Huang KC. 2016. Single-molecule imaging reveals modulation of cell wall synthesis dynamics in live bacterial cells. Nat Commun 7:13170.
23. Dorr T, Moll A, Chao MC, Cava F, Lam H, Davis BM, Waldor MK. 2014. Differential requirement for PBP1a and PBP1b in in vivo and in vitro fitness of Vibrio cholerae. Infect Immun 82:2115-24.
24. Takacs CN, Poggio S, Charbon G, Pucheault M, Vollmer W, Jacobs-Wagner C. 2010. MreB drives de novo rod morphogenesis in Caulobacter crescentus via remodeling of the cell wall. J Bacteriol 192:1671-84.
25. Cava F, de Pedro MA, Lam H, Davis BM, Waldor MK. 2011. Distinct pathways for modification of the bacterial cell wall by non-canonical D-amino acids. EMBO J 30:3442-53.
26. Herrera CM, Henderson JC, Crofts AA, Trent MS. 2017. Novel coordination of lipopolysaccharide modifications in Vibrio cholerae promotes CAMP resistance. Mol Microbiol 106:582-596.
27. Hankins JV, Madsen JA, Giles DK, Brodbelt JS, Trent MS. 2012. Amino acid addition to Vibrio cholerae LPS establishes a link between surface remodeling in gram-positive and gram-negative bacteria. Proc Natl Acad Sci U S A 109:8722-7.
28. Hankins JV, Madsen JA, Giles DK, Childers BM, Klose KE, Brodbelt JS, Trent MS. 2011. Elucidation of a novel Vibrio cholerae lipid A secondary hydroxy-acyltransferase and its role in innate immune recognition. Mol Microbiol 81:1313-29.
29. Mathur J, Davis BM, Waldor MK. 2007. Antimicrobial peptides activate the Vibrio cholerae sigmaE regulon through an OmpU-dependent signalling pathway. Mol Microbiol 63:848-58.
30. Davis BM, Waldor MK. 2009. High-throughput sequencing reveals suppressors of Vibrio cholerae rpoE mutations: one fewer porin is enough. Nucleic Acids Res 37:5757-67.

31. Levin-Reisman I, Ronin I, Gefen O, Braniss I, Shoresh N, Balaban NQ. 2017. Antibiotic tolerance facilitates the evolution of resistance. Science 355:826-830.
32. Ranjit DK, Jorgenson MA, Young KD. 2017. PBP1B Glycosyltransferase and Transpeptidase Activities Play Different Essential Roles during the De Novo Regeneration of Rod Morphology in Escherichia coli. J Bacteriol 199.
33. Malinverni JC, Silhavy TJ. 2009. An ABC transport system that maintains lipid asymmetry in the gram-negative outer membrane. Proc Natl Acad Sci U S A 106:8009-14.
34. Jorgenson MA, Young KD. 2016. Interrupting Biosynthesis of O Antigen or the Lipopolysaccharide Core Produces Morphological Defects in Escherichia coli by Sequestering Undecaprenyl Phosphate. J Bacteriol 198:3070-3079.
35. Yao Z, Kahne D, Kishony R. 2012. Distinct single-cell morphological dynamics under beta-lactam antibiotics. Mol Cell 48:705-12.
36. Dorr T, Lam H, Alvarez L, Cava F, Davis BM, Waldor MK. 2014. A novel peptidoglycan binding protein crucial for PBP1A-mediated cell wall biogenesis in Vibrio cholerae. PLoS Genet 10:e1004433.
37. Hussain S, Wivagg CN, Szwedziak P, Wong F, Schaefer K, Izore T, Renner LD, Holmes MJ, Sun Y, Bisson-Filho AW, Walker S, Amir A, Lowe J, Garner EC. 2018. MreB filaments align along greatest principal membrane curvature to orient cell wall synthesis. Elife 7.
38. Gibson DG, Young L, Chuang RY, Venter JC, Hutchison CA, 3rd, Smith HO. 2009. Enzymatic assembly of DNA molecules up to several hundred kilobases. Nat Methods 6:343-5.
39. Donnenberg MS, Kaper JB. 1991. Construction of an eae deletion mutant of enteropathogenic Escherichia coli by using a positive-selection suicide vector. Infect Immun 59:4310-7.
40. Miller VL, Mekalanos JJ. 1988. A novel suicide vector and its use in construction of insertion mutations: osmoregulation of outer membrane proteins and virulence determinants in Vibrio cholerae requires toxR. J Bacteriol 170:2575-83.
41. Ferrieres L, Hemery G, Nham T, Guerout AM, Mazel D, Beloin C, Ghigo JM. 2010. Silent mischief: bacteriophage Mu insertions contaminate products of Escherichia coli random mutagenesis performed using suicidal transposon delivery plasmids mobilized by broad-host-range RP4 conjugative machinery. J Bacteriol 192:6418-27.
42. Yamaichi Y, Dorr T. 2017. Transposon Insertion Site Sequencing for Synthetic Lethal Screening. Methods Mol Biol 1624:39-49.
43. Pritchard JR, Chao MC, Abel S, Davis BM, Baranowski C, Zhang YJ, Rubin EJ, Waldor MK. 2014. ARTIST: high-resolution genome-wide assessment of fitness using transposon-insertion sequencing. PLoS Genet 10:e1004782.

746 44. Chao MC, Abel S, Davis BM, Waldor MK. 2016. The design and analysis
747 of transposon insertion sequencing experiments. Nat Rev Microbiol
748 14:119-28.
749

A

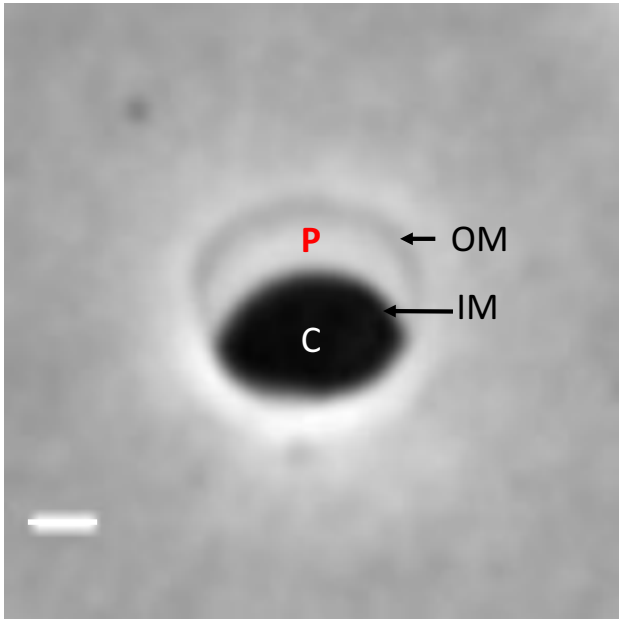

B

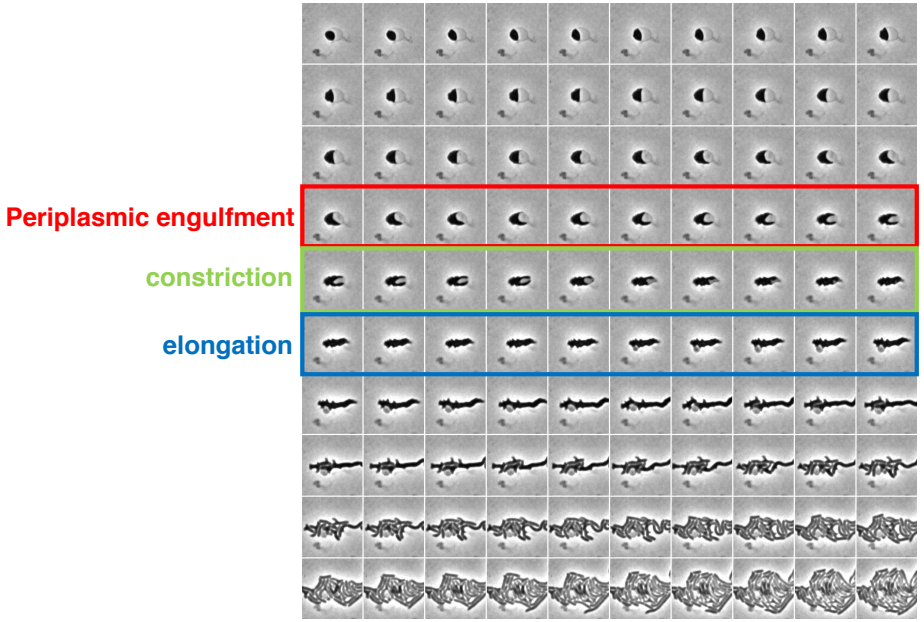

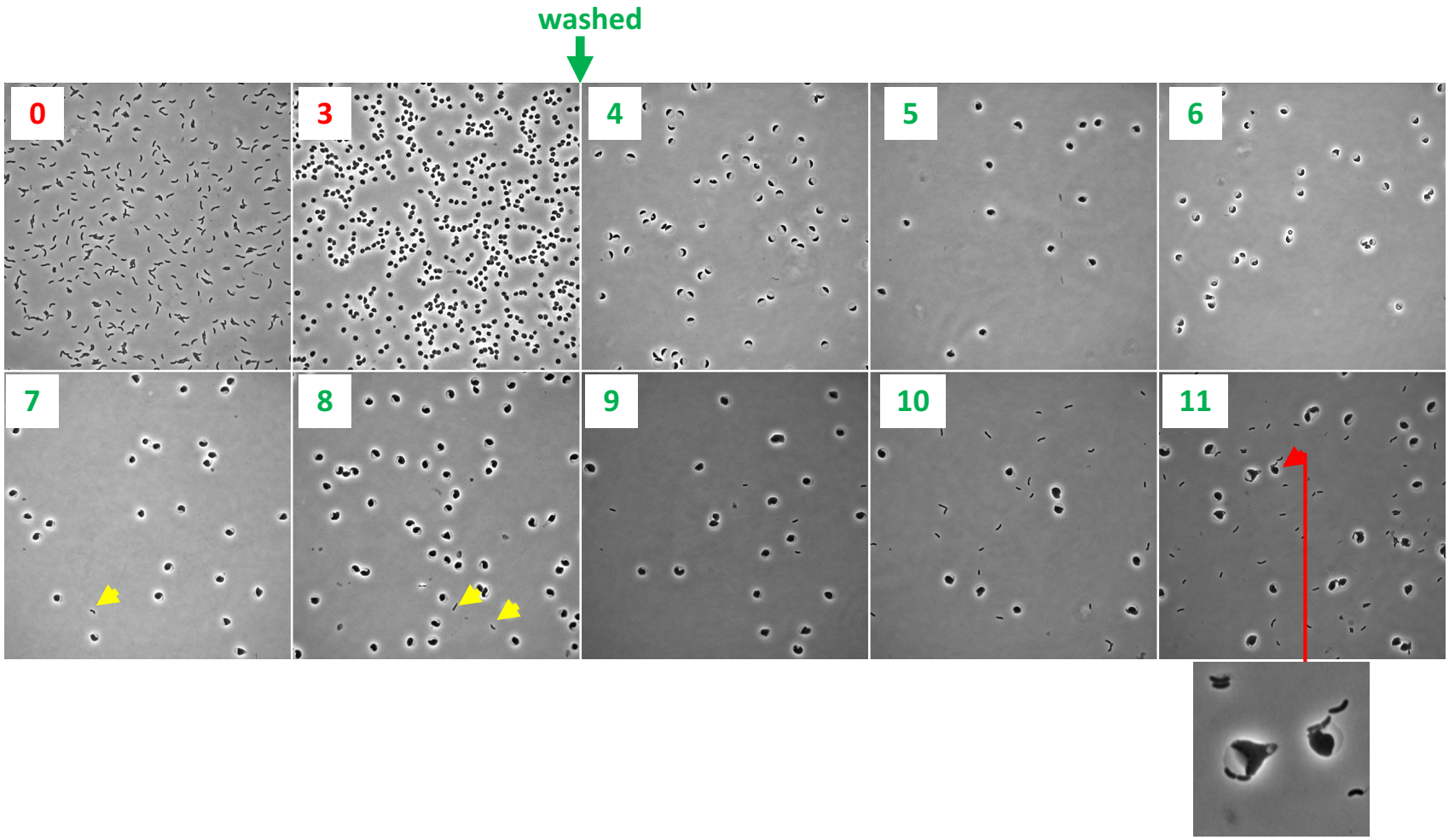
washed
0
3
4
5
6
7
8
9
10
11

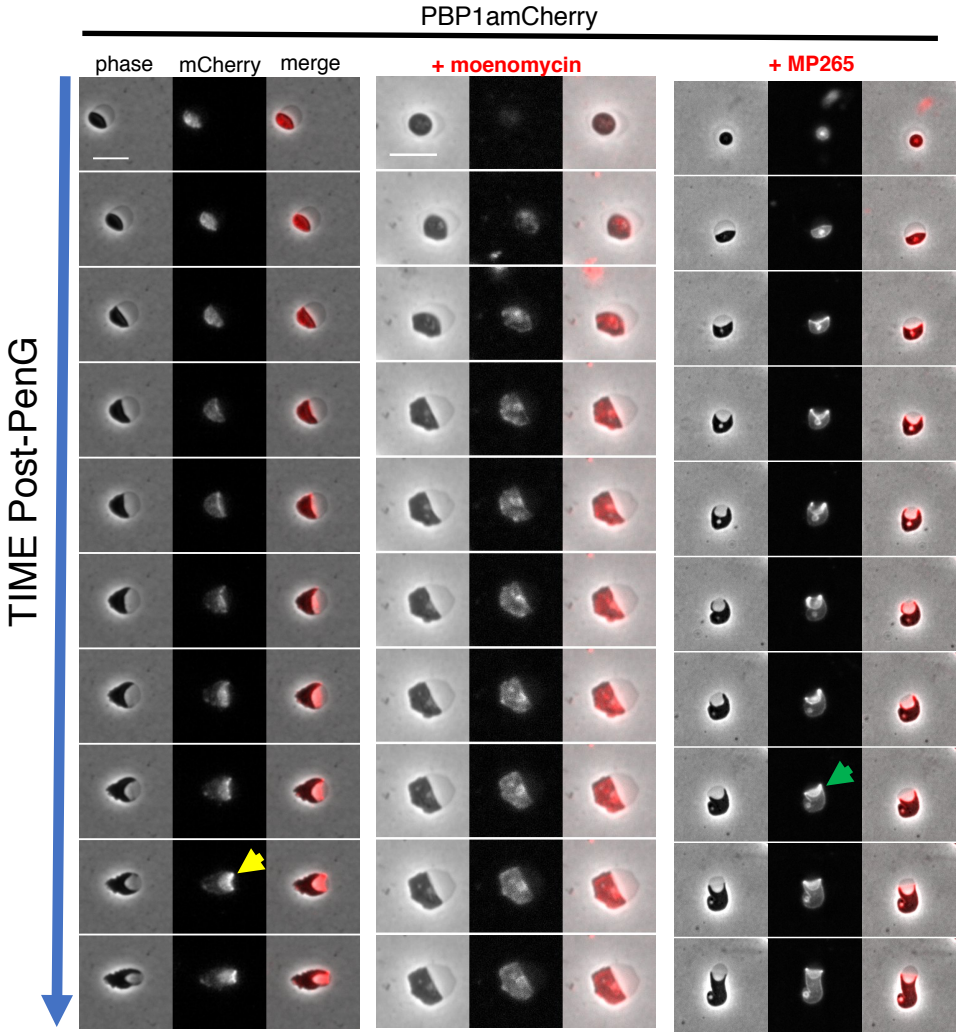
PBP1amCherry
phase
mCherry
merge
+ moenomycin
+ MP265
TIME Post-PenG

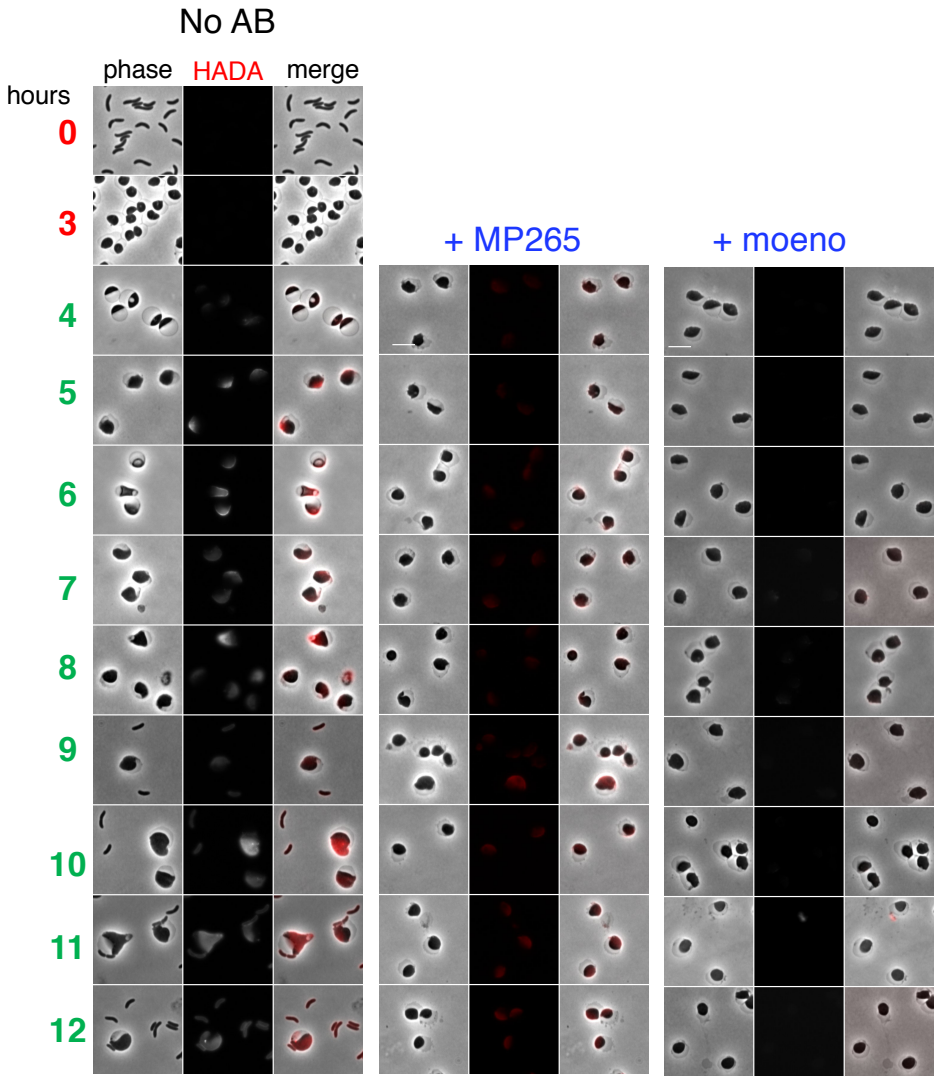
No AB
phase
HADA
merge
hours
0
3
4
5
6
7
8
9
10
11
12
+ MP265
+ moeno

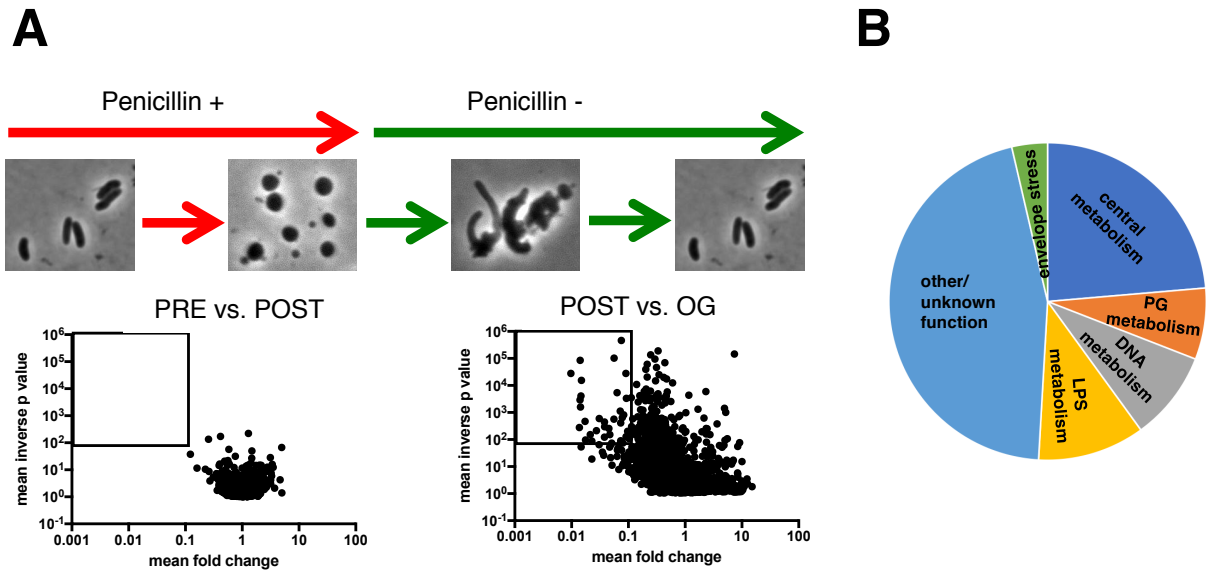
A
Penicillin +
Penicillin -
PRE vs. POST
POST vs. OG
mean inverse p value
mean fold change
0.001
0.01
0.1
1
10
100
B
central metabolism
PG metabolism
DNA metabolism
LPS metabolism
other/ unknown function
envelope stress

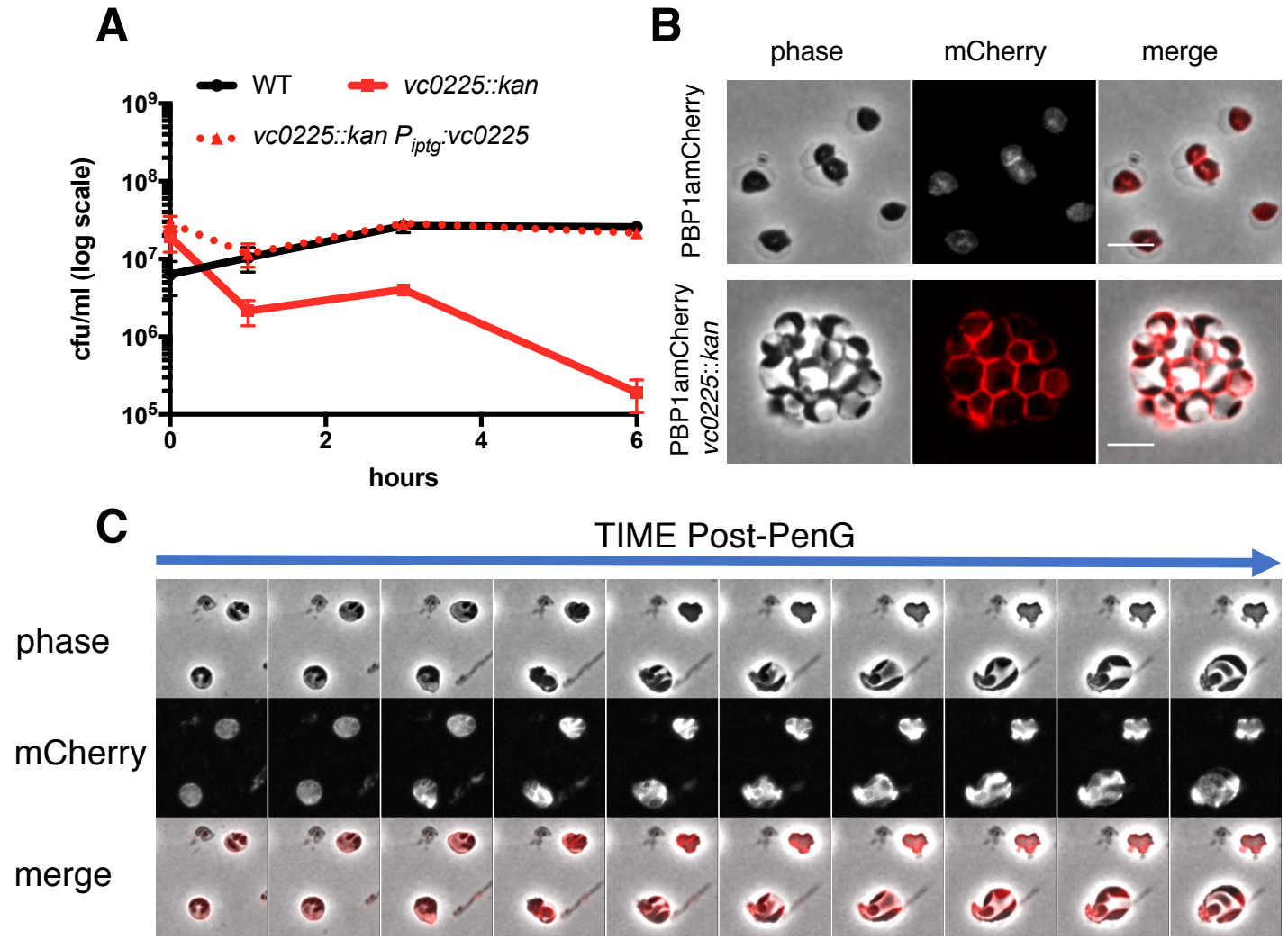
A
WT
vc0225::kan
vc0225::kan P iptg:vc0225
cfu/ml (log scale)
10^9
10^8
10^7
10^6
10^5
0
2
4
6
hours
B
phase
mCherry
merge
PBP1amCherry
PBP1amCherry vc0225::kan
C
TIME Post-PenG
phase
mCherry
merge

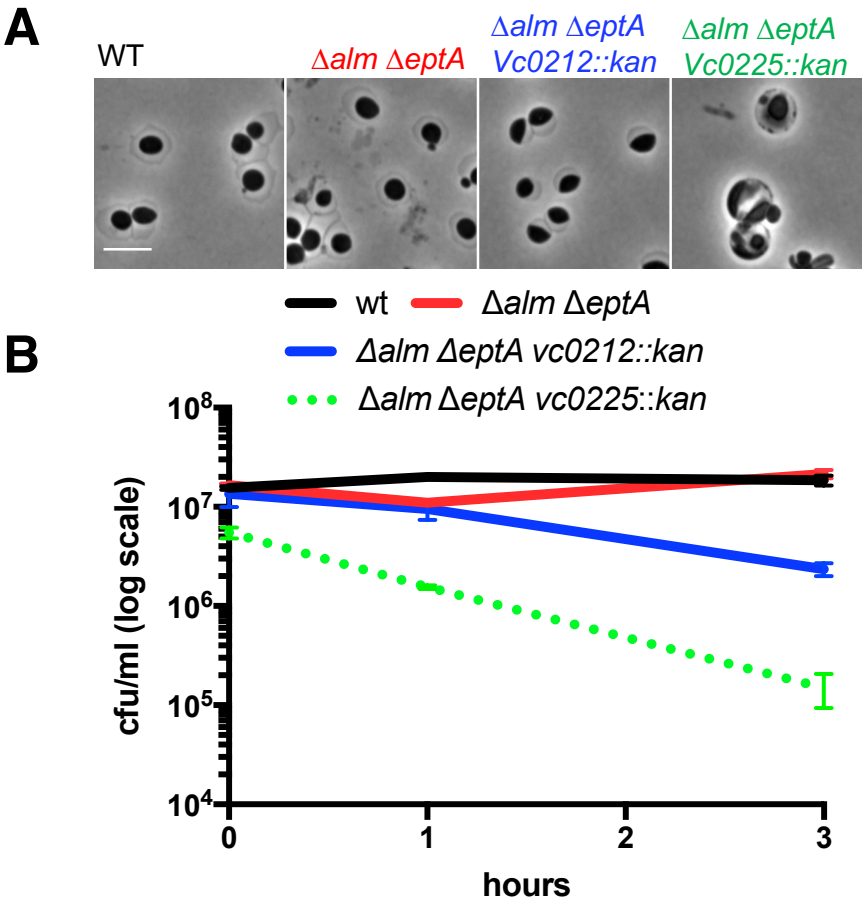
A
WT
Δalm ΔeptA
Δalm ΔeptA Vc0212::kan
Δalm ΔeptA Vc0225::kan
B
wt
Δalm ΔeptA
Δalm ΔeptA vc0212::kan
Δalm ΔeptA vc0225::kan
cfu/ml (log scale)
10^8
10^7
10^6
10^5
10^4
0
1
2
3
hours

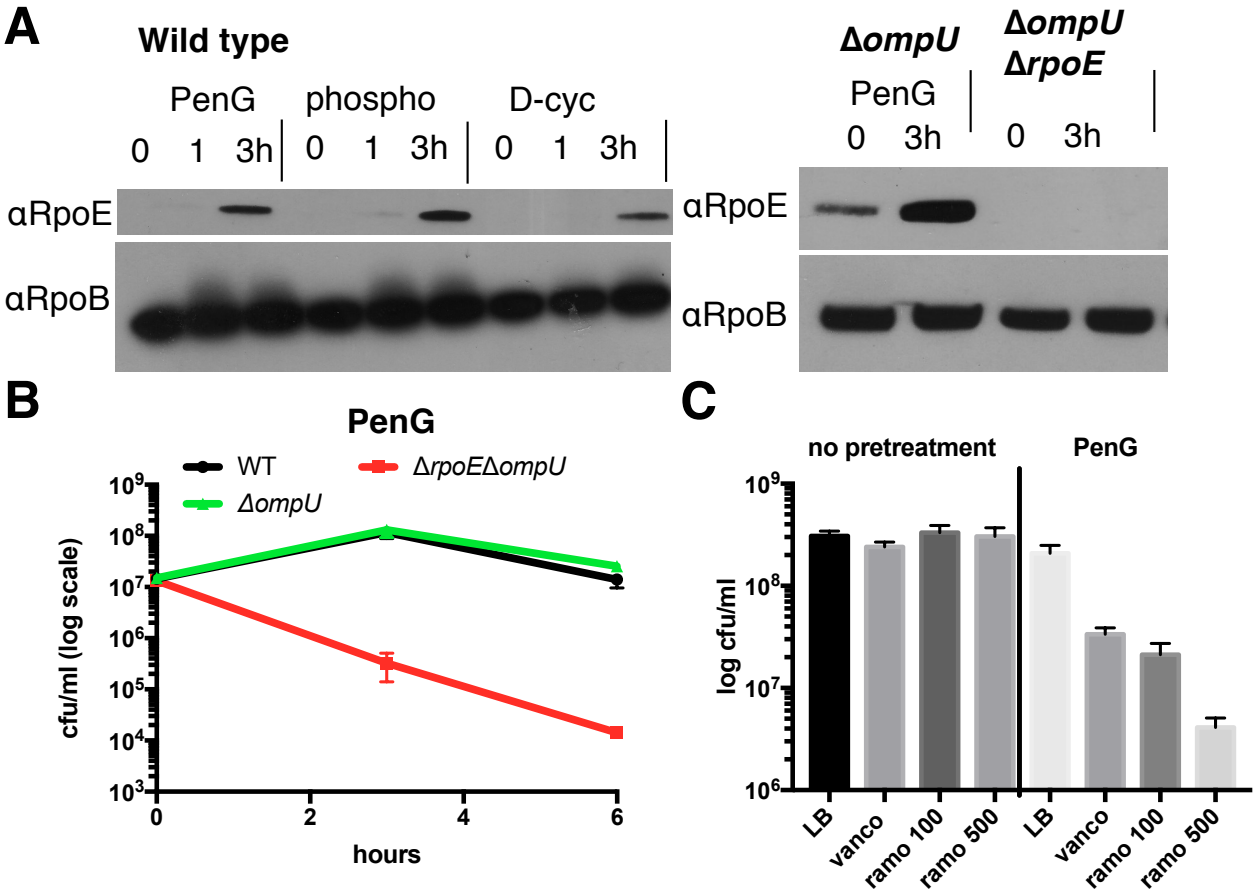
A
Wild type
PenG
phospho
D-cyc
0 1 3h 0 1 3h 0 1 3h
αRpoE
αRpoB
ΔompU
ΔompU ΔrpoE
PenG
0 3h 0 3h
αRpoE
αRpoB
B
PenG
WT
ΔrpoEΔompU
ΔompU
cfu/ml (log scale)
hours
C
no pretreatment
PenG
log cfu/ml
LB
vanco
ramo 100
ramo 500

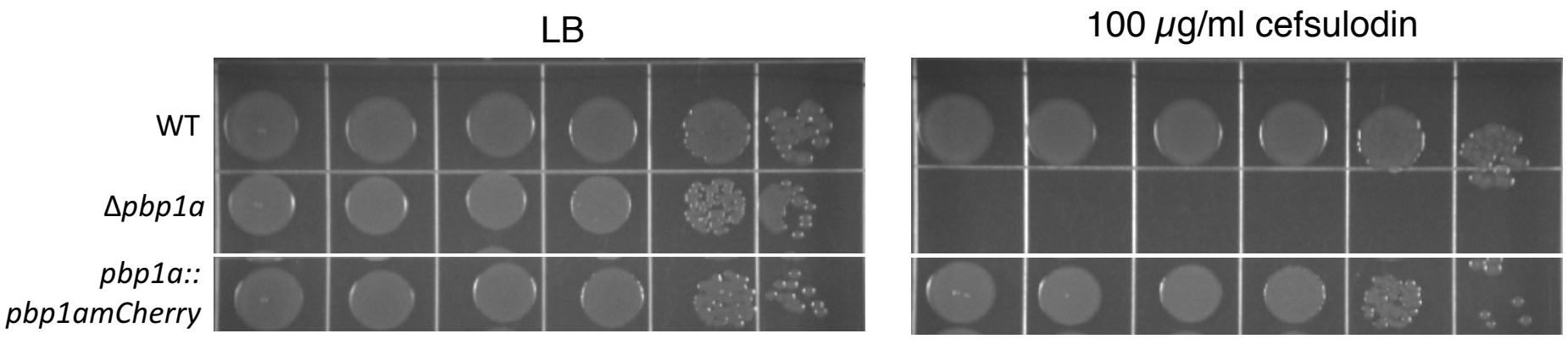
LB
100 μg/ml cefsulodin
WT
Δpbp1a
pbp1a::
pbp1amCherry

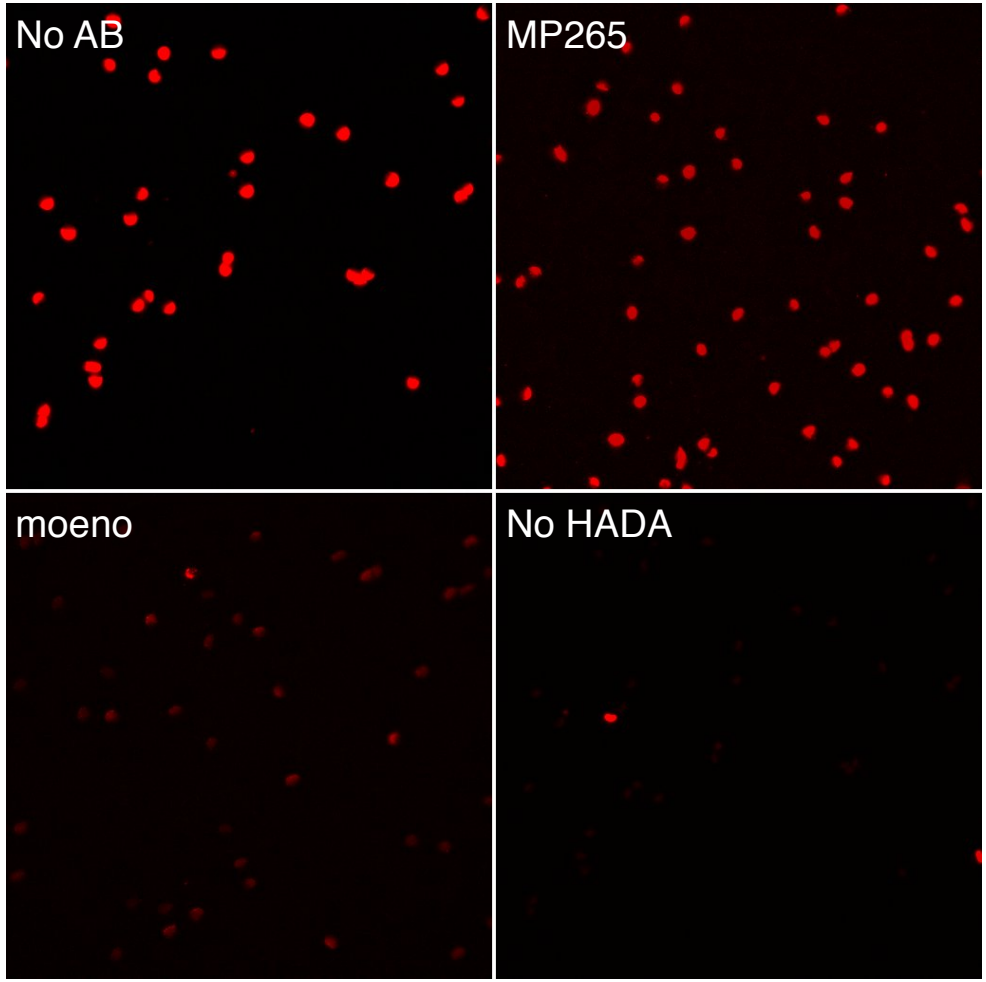
No AB
MP265
moeno
No HADA

gene name	annotation	putative role	fold change
VC_2270	riboflavin synthase subunit alpha	Riboflavin biosynthesis	257
VC_2271	riboflavin-specific deaminase	Riboflavin biosynthesis	139
VC_0724	phosphate ABC transporter permease	Phosphate regulation	121
VC_1716	condensin subunit F	Chromosome condensation	109
VC_2153	D,D-carboxypeptidase-like protein	peptidoglycan metabolism	109
VC_1714	cell division protein MukB	Chromosome condensation	90
VC_0212	lipid A biosynthesis (KDO)2-(lauroyl)-lipid IVA acyltransferase	lipopolysaccharide metabolism	89
VC_1263	GTP cyclohydrolase II/ribA	Riboflavin biosynthesis	86
VC_2312	murein transglycosylase A	peptidoglycan metabolism	85
VC_0374	glucose-6-phosphate isomerase	carbon metabolism	81
VC_1894	hypothetical protein VC1894/LpoB	peptidoglycan metabolism	77
VC_1715	condensin subunit E	Chromosome condensation	57
VC_0761	hypothetical protein VC0761/yfgM	envelope stress response	48
VC_0225	lipopolysaccharide biosynthesis protein	lipopolysaccharide metabolism	40
VC_0851	small protein A/BamE	outer membrane metabolism	40
VC_2635	penicillin-binding protein 1A	peptidoglycan metabolism	39
VC_0908	D,D-heptose 1,7-bisphosphate phosphatase	capsule biosynthesis	38
VC_2465	periplasmic negative regulator of sigmaE	envelope stress response	36
VC_0936	polysaccharide export-like protein	capsule biosynthesis	35
VC_0236	ADP-heptose--LPS heptosyltransferase II	lipopolysaccharide metabolism	33
VC_0289	gluconate utilization system gnt-I transcriptional repressor	carbon metabolism	33
VC_A0647	hypothetical protein VCA0647	unknown	29
VC_0034	thiol:disulfide interchange protein	unknown	29
VC_A0424	hypothetical protein VCA0424/DUF3709	unknown	28
VC_2629	shikimate kinase I	amino acid biosynthesis	27
VC_0370	hypothetical protein VC0370/YdiY	salt-induced OM protein	26
VC_1630	ABC transporter ATP-binding protein/LolD	lipoprotein export	23
VC_1021	LuxO repressor protein	quorum sensing	23
VC_0240	ADP-L-glycero-D-manno-heptose-6-epimerase	lipopolysaccharide metabolism	21
VC_0952	hypothetical protein VC0952/rsfS	ribosome downregulation	19
VC_A0804	ATP-dependent RNA helicase DeaD	RNA metabolism	18
VC_0237	O-antigen ligase waaL	lipopolysaccharide metabolism	18
VC_1039	asmA protein	outer membrane metabolism	18
VC_0984	cholera toxin transcriptional activator	pathogenesis	17
VC_0431	arginine repressor ArgR	amino acid biosynthesis	17
VC_2322	exonuclease V subunit gamma-RecC	DNA recombination and repair	16
VC_A0448	hypothetical protein VCA0448	unknown	15
VC_0547	aspartate kinase	amino acid biosynthesis	15
VC_2298	lipoprotein	unknown	15
VC_1697	Short-chain dehydrogenases/reductases	central metabolism	14
VC_0377	hypothetical protein VC0377/CheX	chemotaxix	14
VC_0346	tRNA delta(2)-isopentenylpyrophosphate transferase	tRNA modification	14
VC_A0645	hypothetical protein VCA0645	unknown	14
VC_0378	zinc uptake regulation protein	metal homeostasis	13
VC_0003	tRNA modification GTPase TrmE	tRNA modification	13
VC_A0344	hypothetical protein VCA0344	unknown	13
VC_A0395	hypothetical protein VCA0395	unknown	13
VC_0632	D-alanyl-D-alanine carboxypeptidase/endopeptidase	peptidoglycan metabolism	11
VC_1682	peptide ABC transporter permease	antimicrobial peptide transport	11
VC_0665	Fis family transcriptional regulator	exopolysaccharide synthesis	11
VC_A0573	DamX-like protein	cell division	11
VC_0223	ADP-heptose--LPS heptosyltransferase II	lipopolysaccharide metabolism	11
VC_0727	transcriptional regulator PhoU	Phosphate regulation	10
VC_2320	exodeoxyribonuclease V/RecB	DNA recombination and repair	10
VC_A0405	hypothetical protein VCA0405	unknown	10
VC_1700	intracellular septation protein A	unknown	10

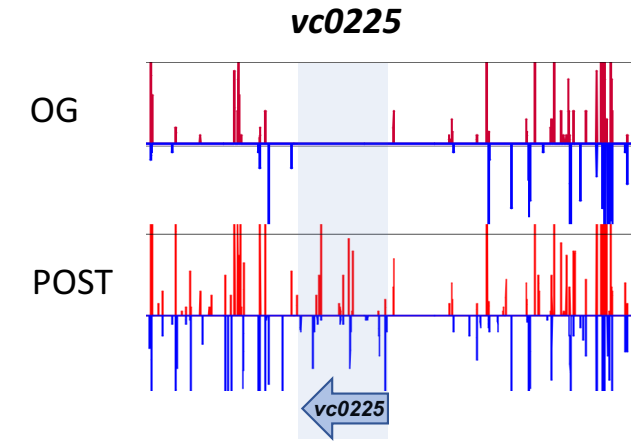

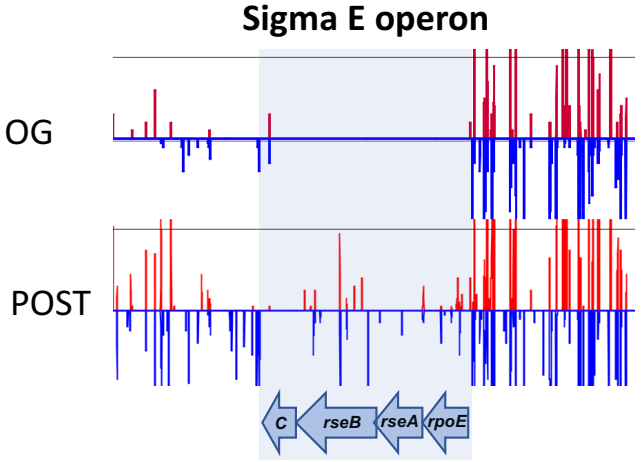

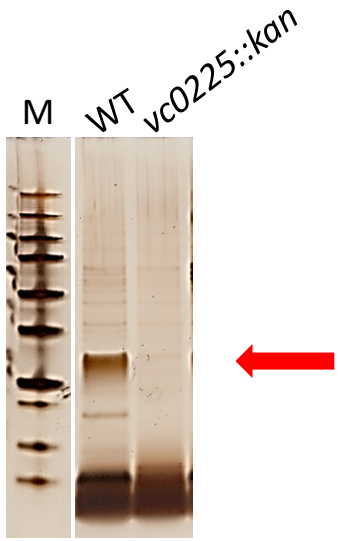
M
WT
vc0225::kan

A

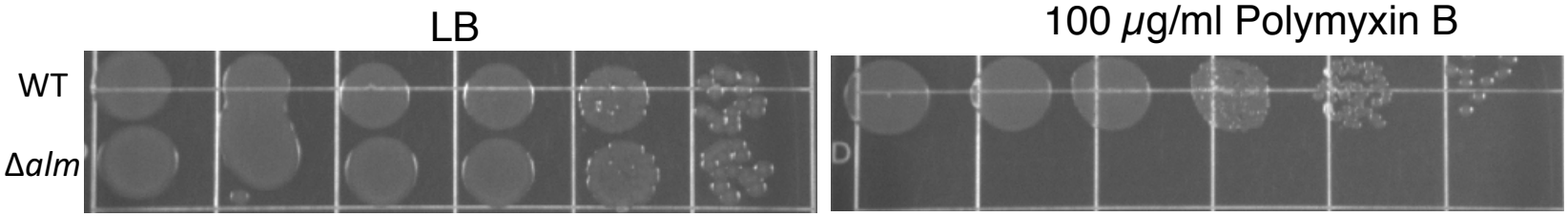
LB
100 μg/ml Polymyxin B
WT
Δalm

B

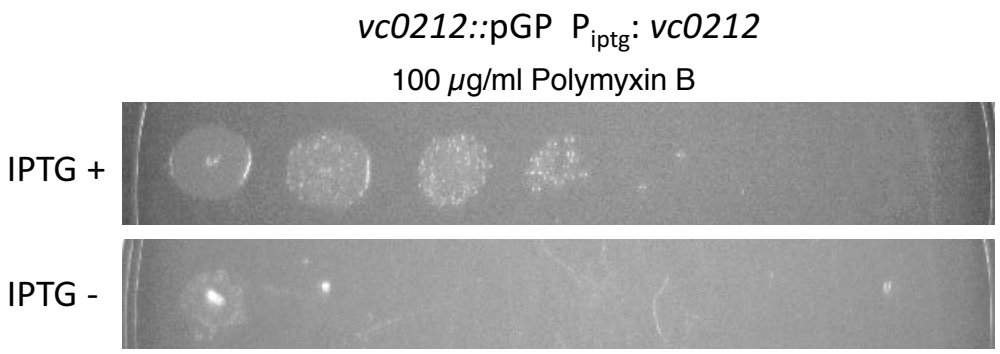
vc0212::pGP Piptg: vc0212
100 μg/ml Polymyxin B
IPTG +
IPTG -